

1 **Remote Energetic Neutral Atom Imaging of Electric Potential Over a Lunar Magnetic**
2 **Anomaly**

3 Y. Futaana^{1*}, S. Barabash¹, M. Wieser¹, C. Lue^{1,2}, P. Wurz³, A. Vorburger³, A. Bhardwaj⁴, K.
4 Asamura⁵

5 ¹Swedish Institute of Space Physics, Box 812, SE-98128 Kiruna, Sweden.

6 ²Department of Physics, Umeå University, Linnaeus väg 24, SE-90187 Umeå, Sweden.

7 ³Physikalisches Institut, University of Bern, Sidlerstrasse 5, CH-3012 Bern, Switzerland.

8 ⁴Space Physics Laboratory, Vikram Sarabhai Space Center, Trivandrum 695 022, India.

9 ⁵Institute of Space and Astronautical Science, 3-1-1 Yoshinodai, Sagami-hara 252-5210, Japan.

10 *Corresponding author: Yoshifumi Futaana (futaana@irf.se)

11 **Abstract.**

12 The formation of electric potential over lunar magnetized regions is essential for understanding
13 fundamental lunar science, for understanding the lunar environment, and for planning human
14 exploration on the Moon. A large positive electric potential was predicted and detected from
15 single point measurements. Here, we demonstrate a remote imaging technique of electric
16 potential mapping at the lunar surface, making use of a new concept involving hydrogen neutral
17 atoms derived from solar wind. We apply the technique to a lunar magnetized region using an
18 existing dataset of the neutral atom energy spectrometer SARA/CENA on Chandrayaan-1.
19 Electrostatic potential larger than +135 V inside the Gerasimovic anomaly is confirmed. This
20 structure is found spreading all over the magnetized region. The widely spread electric potential
21 can influence the local plasma and dust environment near the magnetic anomaly.

22

23 **1. Introduction**

24 The electrostatic potential between the Moon surface and space is a key parameter that is
25 fundamental for lunar science and human exploration on the Moon. Many investigations of
26 electric potential and associated electric fields have been conducted from the surface using solar
27 wind plasma since the Apollo era. Surface potential influences ambient plasma characteristics
28 and electric current, which balances each other to produce an equilibrium state (Whipple, 1981).
29 A large electric potential, sometimes less than 1 kV, was found from electron energy spectra
30 when high energy electrons precipitated onto the lunar surface (Hakelas et al., 2005). The
31 resulting induced current may potentially damage lander components. The surface potential also
32 affects the environment by influencing dust dynamics and vice versa (e.g. Nitter et al., 1998;
33 Stubbs et al., 2011; Garrick-Bethell et al., 2011).

34 On the other hand, a positive potential is not generally very large. For example, Freeman
35 et al. [1973] used in situ measurement of suprathermal ions and found approximately +10V
36 surface potential. Goldstein [1974] used electron data to find the -3 to +5V potential. These
37 results are consistent with theoretical predictions of a few to +20V (e.g. Freeman and Ibrahim,
38 1975). The exception has been found inside the local magnetized regions (magnetic anomalies)
39 on the lunar surface (e.g. Barnes et al., 1971; Hood et al., 1979; Tsunakawa et al., 2010), where a
40 positive electric potential of the order of ~100 V is expected (Saito et al., 2012). Such electric
41 potentials modify the local plasma environment significantly near the anomaly. Evaluating the
42 electrostatic environment near magnetic anomalies is important as a possible candidate of
43 landing site for future lander missions where cosmic ray protections are expected.

44 Energetic neutral atoms (ENAs), neutral atoms with energies more than 10 eV, have been
45 used for diagnostics for plasma and neutral environments. The powerful remote sensing
46 technique has provided the diagnostics with spatial scales from planetary bodies (Futaana et al.,
47 2011) to the Solar System (McComas et al., 2012). In the case of the Moon, the lack of an
48 intrinsic magnetic field (Colburn et al., 1967; Dyal et al., 1974) allows the solar wind to interact
49 directly with the surface, where ENAs are produced. Thus, ENAs provide information about the
50 solar wind access at the lunar surface (Futaana et al., 2006). The lunar ENAs have already been
51 detected by the ENA sensor, CENA (Chandrayaan-1 Energetic Neutral Atoms), on board a lunar
52 orbiter, Chandrayaan-1 (Barabash et al., 2009). These ENAs, composed only of hydrogen, are
53 originally solar wind protons, which are neutralized on and backscattered from the lunar surface
54 (Wieser et al., 2009).

55 The physical mechanism of the backscattered ENA generation at the lunar surface is not
56 fully understood. The biggest unknown is what causes the high backscattering fraction of 10–
57 20% of impinging solar wind proton flux (Wieser et al., 2009; McComas et al., 2009; Rodríguez
58 et al., 2012; Futaana et al., 2012). The observations contradict with classical understandings of
59 full (<0.1%) absorption (e.g. Behrisch and Wittmaack, 1991; Feldman et al., 2000; Crider and
60 Vondrak, 2002) because of the high porosity of the surface. Another unexplained signature is the
61 ENA energy spectrum. The observed energy spectrum of the backscattered ENAs follows the
62 Maxwell-Boltzmann distribution function with the characteristic energy, i.e. the temperature of
63 the distribution, ranging from 60 to 140 eV. A Maxwell-Boltzmann distribution implies a state of
64 thermal equilibrium, but it is unrealistic to assume equilibrium with such a high temperature (100
65 eV corresponds to 1.16×10^6 K) at the surface. Moreover, the characteristic energy depends only
66 on the solar wind energy; actually, the observation exhibits a linear correlation with the solar

67 wind velocity (Futaana et al., 2012). From classical theory of elastic scattering (e.g. Niehus et al.,
68 1993) linearity with the incident energy (i.e. the solar wind energy) is expected. From these
69 perspectives, an adaption of laboratory knowledge and theoretical understandings of the
70 backscattered process to the situation of a regolith surface in space is needed.

71 Even though the observed characteristics of the backscattered ENAs are not yet fully
72 explained by present theory, we propose here a new empirical method to derive the lunar surface
73 potential from observed hydrogen ENA energy spectra. In this paper, we first describe a new
74 method to map the surface electrostatic potential. Then, we apply this method to available
75 observations near a magnetic anomaly to show a large potential generation over a wide range of
76 the magnetic anomaly. We also discuss the result and its influence on surface plasma and dust
77 environments and human activities.

78 **2. Mapping method of electric potential**

79 Assuming the existence of a surface potential ($\pm\Phi_{surf}$) between the lunar surface and
80 space (solar wind), the solar wind will be decelerated (or accelerated) before reaching the
81 surface. The solar wind energy at the surface becomes $E_{surf}=E_{sw}-(\pm\Phi_{surf})$, where E_{sw} is the
82 original solar wind energy. When the decelerated (or accelerated) solar wind is backscattered as
83 ENAs, the generated ENA temperature, T_{ena} , is determined only from the solar wind energy at
84 the lunar surface, E_{surf} (Futaana et al., 2012). Because T_{ena} is a measurable quantity, we can
85 determine E_{surf} . The difference between E_{surf} and E_{sw} provides the surface potential, $\pm\Phi_{surf}$.

86 For this method, it is important to produce a proper reference model, i.e., the relationship
87 between E_{sw} and T_{ena} for uncharged surface. We here use a model derived from more than 100
88 CENA observations in the equatorial region (Futaana et al., 2012):

$$T_{ena} = V_{sw} \cdot 0.273 - 1.99$$

where T_{ena} is measured in eV and V_{sw} is the solar wind velocity in km/s. This can be rewritten as:

$$E_{sw} = \frac{(T_{ena} + 1.99)^2}{14.19} \quad (\text{eq.1})$$

where E_{sw} is also measured in eV. This reference model is derived empirically. No theoretical assurance is yet provided. Here we estimated a statistical uncertainty using the dataset in Futaana et al. [2012] and calculated the ambiguity of the current reference model (eq1) to be -45 and +35 eV (as 25% and 75% percentiles, respectively). Note that the reference model is made using the nominal dayside measurements near the equator. Because no strong magnetic anomalies exist near the equator, the reference model is not affected by magnetic anomalies. On the other hand, the reference model does not account for the surface potential in the nominal dayside conditions. In the nominal dayside, the ultraviolet and electron illumination on the surface produces a potential of a few eV (Vondrak et al., 1983; Němčec et al., 2011). We assume in the following analysis that the surface potential in the nominal state is negligible compared with that in the magnetic anomaly. Our results show that this assumption is realistic.

This new method relies on only the energy spectrum of ENAs. Therefore, it complements classical methods using energy spectra of charged particles. Advantageously, the new method provides an electrostatic potential map. Obviously, when a proper reference model is found, this method can be applied to other airless bodies as Mercury, asteroids and Galileo moons.

3. Application to magnetized region

We applied the above described electric potential mapping method to the region over a lunar magnetic anomaly called Gerasimovic (Fig. 1A). While there are many magnetized regions on the Moon (Tsunakawa et al., 2010), the Gerasimovic is an isolated anomaly, and therefore, it

112 is suitable for a dedicated analysis and discussion (Vorburger et al., 2012). We used the data
113 obtained from the CENA sensor on the Chandrayaan-1 spacecraft over 8 non-consecutive orbits
114 from 16 June 22:06 to 18 June 00:28, 2009. The Moon was located in the solar wind. From
115 WIND/SWE observations, the solar wind is stable (density is $\sim 6 \text{ cm}^{-3}$ and the velocity is ~ 300
116 km s^{-1}).

117 As seen in the ENA flux map (Fig. 1B), there are three characteristic regions (Wieser et
118 al., 2010) from the ENA flux (a) outside the anomaly, (b) enhanced region and (c) inside the
119 anomaly. Outside the anomaly, the ENA flux depends on, to the first order, the cosine of the
120 solar zenith angle, as the solar wind flux at the surface does. It corresponds to the drops in ENA
121 flux at high latitudes (Fig. 1B). For the electrostatic potential map (Fig. 1A), a clear signature
122 with a positive potential of $>150 \text{ V}$ is found inside the anomaly. The potential structure spread
123 over the majority of the magnetized area. In contrast, in the enhanced region and outside the
124 anomaly, no potential structures were found. Small-scale potential structures (below -100 or
125 above 100 V) are most likely artificial, because the spatial scale of them is comparable to the
126 dimension of the sensor FOV projection ($\sim 1^\circ$ in latitude and $\sim 8^\circ$ in longitude).

127 Outside the anomaly, the characteristic energy of backscattered ENA is 84.3 eV (Fig. 2).
128 Using the reference model (eq.1), the corresponding solar wind energy is found to be 525 eV . In
129 the enhanced region, the ENA flux is higher than in the other regions, and the ENA temperature
130 inside the enhanced region does not change (83.3 eV), indicating that the solar wind energy at
131 the surface of the enhanced region is 512 eV . Inside the magnetic anomaly, the ENA
132 characteristic energy is 72.5 eV , and the derived solar wind energy at the surface is 390 eV . The
133 difference in the solar wind energy between the outside (525 eV) and inside of the anomaly (390

134 eV) is 135 eV, which corresponds to the deceleration of the solar wind by electrostatic potential
135 above the magnetic anomaly.

136 The feature of above energy spectra, namely lower characteristic energy above
137 magnetized region, is commonly seen in the CENA dataset. Therefore, this empirical method of
138 electric potential derivation could also work for other magnetic anomalies, in which the surfaces
139 are positively charged.

140 **4. Discussion**

141 The positive potential formed above a magnetic anomaly is expected based on the charge
142 separation theory. Ions can penetrate farther than electrons in the interaction region, and the
143 charge separation produces an outward-facing electric field. Recently, Saito et al. [2012]
144 demonstrated that the *in situ* measurements of the energy spectra for solar wind protons, alpha
145 particles and electrons at 30 km altitude are consistently explained if one assumes the presence
146 of a +150 V electric potential inside the magnetic anomaly. These authors analyzed a different
147 anomaly (South Pole Aitken), but their electric potential is in a good agreement with our result of
148 135 V electric potential formation.

149 We emphasize here that we do not see any strong electric potential in the enhanced
150 region of the magnetic anomaly. The enhanced region can be attributed to an increase in the solar
151 wind proton flux at the lunar surface caused the deflection of the ion flow above the magnetic
152 anomaly (Wieser et al., 2010). The deflection magnifies the net solar wind flux of the enhanced
153 region, similar to the Earth's magnetosheath. However, the lack of electrostatic potential in the
154 enhanced region indicates that there is no electric potential formed above the enhanced region.
155 Therefore, the deflection above the anomaly is mainly caused by magnetic forces, and the

156 previously suggested mini-scale bow shock (Lin et al., 1998) is evidently not formed above the
157 magnetic anomaly.

158 The large electric potential influences the near-surface environment near the magnetic
159 anomaly. It explains the observed signatures of solar wind ion reflection that are correlated with
160 the magnetic anomaly (Lue et al., 2011). A high electric potential not only decelerates the
161 incoming solar wind protons but also thermalizes the plasma and partially reflects the protons
162 (Saito et al., 2012) as illustrated in Fig. 3. This also modifies the lunar dust environment because
163 charged dust particles are lifted and transported by this large electric potential. Recently, the
164 differentiation of dust by a large electric potential was proposed (Garrick-Bethell et al., 2011;
165 Wang et al., 2012) to explain the coincidence of the magnetic anomalies and the coinciding
166 characteristic albedo signatures (swirls). Our finding of a large positive electric potential
167 structure all over the Gerasimovic anomaly supports the hypothesis of coinciding swirl
168 formation.

169 Despite its effects on the near-surface environment, this relatively large electrostatic
170 potential above the magnetic anomaly does not pose any significant challenges for human and
171 robotic activities on the Moon. The widely spread electric potential structure over the magnetized
172 region suggests a relatively weak electric field. For example, assuming a 150V electrostatic
173 potential along 200 km, the corresponding electric field is 0.8 mV/m, which is of the same order
174 of the solar wind convection electric field at 1 AU. The vertical field could be stronger: If we
175 assume 10 km, the electric field could be 15 mV/m. This is still not strong enough to influence
176 the human and robotic activities directly, for example discharging at the lunar surface. Therefore,
177 a region under a magnetic anomaly still can be a good candidate site for landing and future
178 exploration of the Moon. Secondary effects, such as dust levitation due to the electric field and

179 its adsorption to any components (Stubbs et al., 2007), should be carefully assessed for robotic
180 activities, but such effects are commonly observed everywhere on the Moon.

181 **Acknowledgments**

182 This work was supported by funding from the Swedish National Space Board (SNSB) in
183 Sweden. We thank the WIND/SWE team for providing the solar wind data.

184

185 **Reference**

186 Archinal, B. A., M. R. Rosiek, R. L. Kirk, and B. L. Redding, "The united lunar control network
187 2005" (U.S. Geological Survey Open-File Report, 2006-1367, 2005).

188 Barabash, S. et al., Investigation of the solar wind-Moon interaction on board Chandrayaan-1
189 mission with the SARA experiment, *Current Science*, **96** (4), 526-532 (2009).

190 Barnes, A., P. Cassen, J. D. Mihalov, A. Eviatar, Permanent lunar surface magnetism and its
191 deflection of the solar wind, *Science*, **172**(3984), 716–718, (1971).

192 Behrisch, R., K. Wittmaack, in *Sputtering by Particle Bombardment III*, R. Behrisch and K.
193 Wittmaack, Eds. (Springer-Verlag, New York, 1991), pp. 1-13.

194 Colburn, D. S., R. G. Currie, J. D. Mihalov, C. P. Sonett, Diamagnetic Solar-Wind cavity
195 discovered behind moon, *Science*, **158**(3804), 1040–1042, (1967).

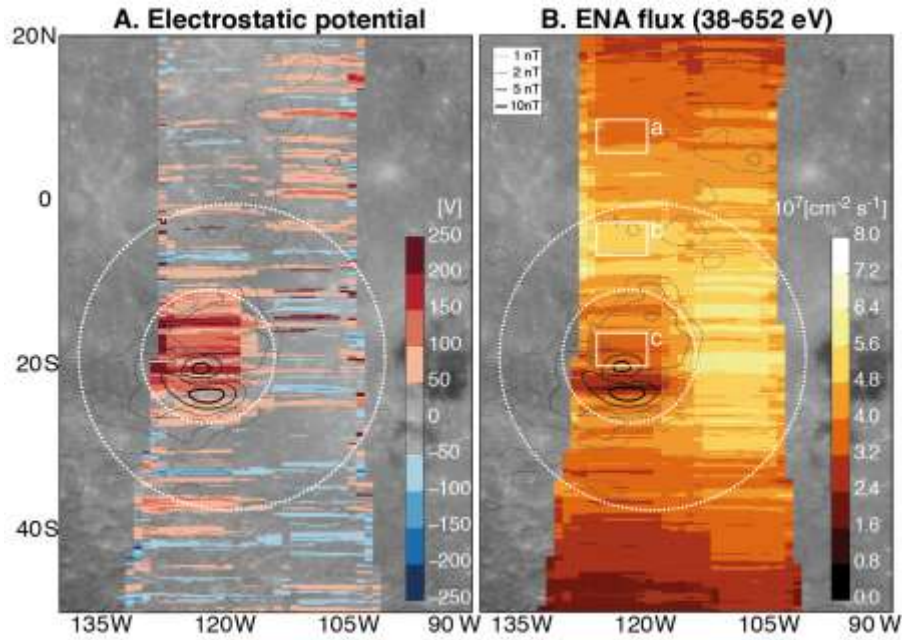
196 Crider, D. H., R. R. Vondrak, Hydrogen migration to the lunar poles by solar wind bombardment
197 of the moon, *Adv. Space Res.*, **30** (8), 1869-1874 (2002).

198 Dyal, P., C. W. Parkin, W. D. Daily, Magnetism and the interior of the Moon, *Rev. Geophys.*, **12**
199 (4), 568-591 (1974).

- 200 Feldman, W. C., et al., Polar hydrogen deposits on the Moon, *J. Geophys. Res.*, **105** (E2), 4175-
201 4195 (2000).
- 202 Freeman, J. W., M. A. Fenner and H. K. Hills, Electric potential of the Moon in the solar wind, *J.*
203 *Geophys. Res.*, **78**, 4560-4567 (1973).
- 204 Freeman, Jr., J. W., M. Ibrahim, Lunar electric fields, surface potential and associated plasma
205 sheaths, *The Moon*, **14**, 103-114 (1975).
- 206 Futaana, Y., S. Barabash, M. Holmström, and A. Bhardwaj, Low energy neutral atoms imaging
207 of the Moon, *Planet. Space Sci.*, **54** (2), 132-143 (2006).
- 208 Futaana, Y. et al., Exospheres and energetic neutral atoms of Mars, Venus and Titan, *Space Sci.*
209 *Rev.*, **162**, 213-266, (2011).
- 210 Futaana, Y. et al., Empirical energy spectra of neutralized solar wind protons from the lunar
211 regolith, *J. Geophys. Res.*, **117**, doi:10.1029/2011JE004019 (2012).
- 212 Garrick-Bethell, I., J. W. Head III, C. M. Pieters, Spectral properties, magnetic fields, and dust
213 transport at lunar swirls, *Icarus*, **212** (2), 480-492 (2011).
- 214 Goldstein, B. E., Observations of electrons at the lunar surface, *J. Geophys. Res.*, **79** (1), 23-35
215 (1974).
- 216 Halekas, J. S., R. P. Lin, D. L. Mitchell, Large negative lunar surface potentials in sunlight and
217 shadow, *Geophys. Res. Lett.*, **32**, doi: 10.1029/2005GL022627 (2005).
- 218 Hood, L. L., P. J. Coleman, Jr., D. E. Wilhelms, Lunar nearside magnetic anomalies, in *Lunar*
219 *and Planetary Science Conference Proceedings*, N. W. Hinners, Eds., vol. 10, pp. 2235-
220 2257 (1979).

- 221 Lin, R. P., et al., Lunar Surface Magnetic Field and Their Interaction with the Solar Wind:
222 Results from Lunar Prospector, *Science*, **281**, 1480-1484, 1998.
- 223 Lue, C., et al., Strong influence of lunar crustal fields on the solar wind flow, *Geophys. Res.*
224 *Lett.*, **38** (3), doi: 10.1029/2010GL046215 (2011).
- 225 McComas, D. J., et al., Lunar backscatter and neutralization of the solar wind: First observations
226 of neutral atoms from the Moon, *Geophys. Res. Lett.*, **36** (12), doi: 10.1029/2009GL038794
227 (2009).
- 228 McComas, D. J., et al., The heliosphere's interstellar interaction: No bow shock. *Science*, **336**
229 (6086), 1291–1293 (2012).
- 230 Niehus, H., W. Heiland, E. Taglauer, Low-energy ion scattering at surfaces, *Surface Science*
231 *Reports*, **17** (4-5), 213-303 (1993).
- 232 Nitter, T., O. Havnes, F. Melandso, Levitation and dynamics of charged dust in the photoelectron
233 sheath above surface in space, *J. Geophys. Res.*, **103** (A4), 6605–6620 (1998).
- 234 Němčec, Z., et al., Lunar dust grain charging by electron impact: Dependence of the surface
235 potential on the grain size. *Ap. J.*, **738** 1, doi: 10.1088/0004-637X/738/1/14 (2011).
- 236 Purucker, M. E., J. B. Nicholas, Global spherical harmonic models of the internal magnetic field
237 of the moon based on sequential and coestimation approaches, *J. Geophys. Res.*, **115** (E12),
238 doi: 10.1029/2010JE003650 (2010).
- 239 Rodríguez M., D. F. et al., IBEX-Lo observations of energetic neutral hydrogen atoms
240 originating from the lunar surface, *Planet. Space Sci.*, **60** (1), 297-303 (2012).
- 241 Saito, Y. et al., Simultaneous observation of the electron acceleration and ion deceleration over
242 lunar magnetic anomalies, *Earth Planets Space*, **64**, 83-92 (2012).

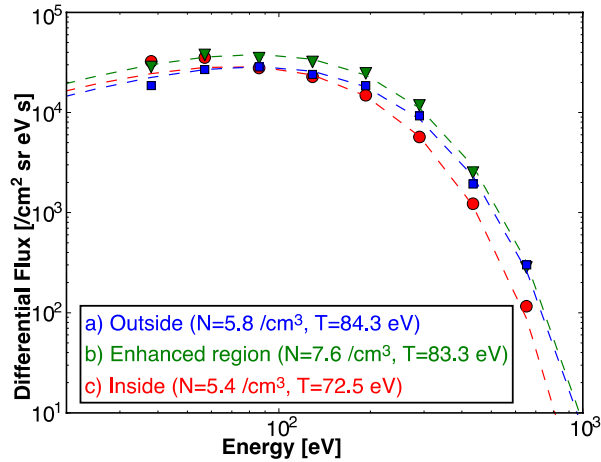
- 243 Stubbs, T. J., R. R. Vondrak, W. M. Farrell, *Impact of dust on lunar exploration*. in Dust in
244 Planetary Systems, H. Krüger, A. L. Graps, A.L. Eds., SP-643. ESA Publications, pp. 239–
245 244 (2007).
- 246 Stubbs, T. J., D. A. Glenar, W. M. Farrell, R. R. Vondrak, M. R. Collier, J. S. Halekas, G. T.
247 Delory, On the role of dust in the lunar ionosphere. *Planet. Space Sci.*, **59** (13), 1659-1664
248 (2011).
- 249 Tsunakawa, H., et al., Lunar magnetic field observation and initial global mapping of lunar
250 magnetic anomalies by MAP-LMAG onboard SELENE (Kaguya), *Space Sci. Rev.*, **154** (1-
251 4), 219-251 (2010).
- 252 Vondrak, R. R., Lunar base activities and the lunar environment, in *2nd Conference on Lunar*
253 *Bases and Space Activities*, (NASA, Johnson Space Center, 1983), pp. 337-345.
- 254 Vorburger, A., et al., Energetic neutral atom observations of magnetic anomalies on the lunar
255 surface, *J. Geophys. Res.*, **117** (A7), doi: 10.1029/2012JA017553 (2012).
- 256 Wang, X. M. Hornyi, S. Robertson. Characteristics of a plasma sheath in a magnetic dipole field:
257 Implications to the solar wind interaction with the lunar magnetic anomalies, *J. Geophys.*
258 *Res.*, **117**(A6), doi:10.1029/2012JA017635 (2012).
- 259 Whipple, E. C., Potentials of surfaces in space. *Rep. Prog. Phys.* **44**, 1197–1250 (1981).
- 260 Wieser, M. et al., Extremely high reflection of solar wind protons as neutral hydrogen atoms
261 from regolith in space, *Planet. Space Sci.*, **57**, 2132-2134 (2009).
- 262 Wieser, M., et al., First observation of a mini-magnetosphere above a lunar magnetic anomaly
263 using energetic neutral atoms, *Geophys. Res. Lett.*, **37** (5), doi: 10.1029/2009GL041721
264 (2010).



266

267 **Fig. 1.** (A) Map of the electrostatic potential near the Gerasimovic magnetic anomaly. Color
 268 scale shows the electrostatic potential with respect to the solar wind. Two dashed circles separate
 269 the regions inside magnetic anomaly, the enhanced region and the region outside the anomaly.
 270 (B) Map of the ENA flux integrated over 38–652 eV. Similar to the signatures in the integral flux
 271 over 150–600 eV reported previously (Wieser et al., 2010), three regions can be distinctly
 272 identified. Labeled white boxes indicate the areas that produce the energy spectra shown in Fig.
 273 2. The Moon images are from the Clementine grayscale albedo map (Archinal et al., 2005). The
 274 contour lines represent the strength of the modeled magnetic field of anomalies at 30 km altitude
 275 (Purucker and Nicholas, 2010).

276



277

278

Fig. 2 (Figure corrected). Energy spectra of the backscattered ENAs from three characteristic

279

regions. The blue, green and red lines correspond to the backscattered ENAs from a) outside the

280

anomaly, b) the enhanced region and c) inside the anomaly, respectively (Fig. 1B). The symbols

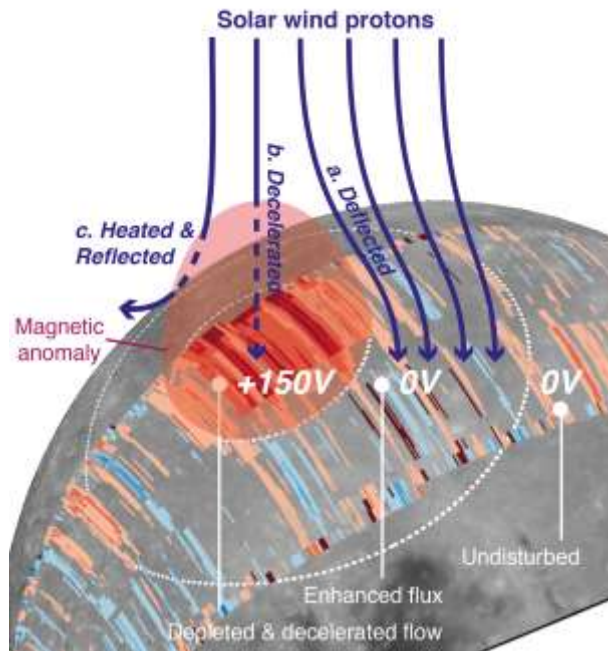
281

show the flux observed by the CENA sensor for each region, and the dashed lines illustrate the

282

best fit by the Maxwell-Boltzmann distributions.

283



284

285 **Fig. 3.** An illustration of the solar wind interaction with the lunar magnetic anomaly. Blue lines
 286 are solar wind proton streamlines modified by the interaction with the magnetic anomaly. The
 287 consequences of the incoming solar wind protons are: a) deflected and reached the enhanced
 288 region without a change in velocity, b) decelerated inside the magnetic anomaly due to the
 289 potential structure of +150V and reached inside magnetic anomaly, or c) heated and reflected in
 290 space before reaching the lunar surface.

291

